Mechanism of Universal Conductance Fluctuations

V. V. Brazhkin, I. M. Suslov
Institute for High Pressure Physics, 108840 Troitsk, Moscow, Russia
P.L.Kapitza Institute for Physical Problems, 119334 Moscow, Russia

Universal conductance fluctuations are usually observed in the form of aperiodic oscillations in the magnetoresistance of thin wires as a function of the magnetic field B. If such oscillations are completely random at scales exceeding ξ_B, their Fourier analysis should reveal a white noise spectrum at frequencies below ξ_B^{-1}. Comparison with the results for 1D systems suggests another scenario: according to it, such oscillations are due to the superposition of incommensurate harmonics and their spectrum should contain discrete frequencies. An accurate Fourier analysis of the classical experiment by Washburn and Webb reveals a purely discrete spectrum in agreement with the latter scenario. However, this spectrum is close in shape to the discrete white noise spectrum whose properties are similar to a continuous one.

Universal conductance fluctuations [1–4] are usually observed in the form of aperiodic oscillations in the magnetoresistance of thin wires as a function of the magnetic field B [5] (Fig. 1) (see [6, 7] for review). According to the theory [1–4], the conductance $G(B)$ at a given magnetic field B undergoes fluctuations of the order of e^2/h under the variation of the impurity configuration; fluctuations in $G(B)$ and $G(B+\Delta B)$ are statistically independent if ΔB exceeds a certain characteristic scale ξ_B. It is reasonable to expect that oscillations in $G(B)$ are completely random at scales exceeding ξ_B. Then, their Fourier analysis should reveal a white noise spectrum (i.e., frequency-independent plateau) at frequencies below ξ_B^{-1}.

Comparison with the results for 1D systems [8] suggests another scenario. A magnetic field perpendicular to a thin wire creates a quadratic potential along this wire [9], which effectively restricts the length of the system L; hence, the variation of the magnetic field is similar to the variation of L. The resistance ρ of a one-dimensional system is a strongly fluctuating quantity and the form of its distribution function $P(\rho)$ strongly depends on first several moments. Indeed, the Fourier transform of $P(\rho)$ specifies the characteristic function

$$F(t)=\left\langle e^{i\rho t}\right\rangle=\sum_{n=0}^{\infty}\frac{(it)^n}{n!}\left\langle\rho^n\right\rangle\,, \qquad (1)$$

which is the generating function of the moments $\langle\rho^n\rangle$. If all moments of the distribution are known, the function $F(t)$ can be constructed using them, and the function $P(\rho)$ is then determined by the inverse Fourier transform. If an increase in the moments $\langle\rho^n\rangle$ with n is not too fast, the contributions of higher moments are suppressed by a factor of $1/n!$, whereas first several moments are significant. These moments are oscillating functions of L,

$$\begin{aligned}\langle\rho\rangle &= a_1(L)+b_1(L)\cos(\omega_1 L+\varphi_1), \qquad (2)\\ \left\langle\rho^2\right\rangle &= a_2(L)+b_2(L)\cos(\omega_2 L+\varphi_2)+\\ &+b_3(L)\cos(\omega_3 L+\varphi_3)\,,\quad \text{etc.},\end{aligned}$$

where $a_k(L)$ and $b_k(L)$ are monotonic functions. The reason is that the growth exponent for $\langle\rho^n\rangle$ is determined by the $(2n+1)$th order algebraic equation (see Appendix), one of whose root is always real, whereas the other roots are complex for energies in the allowed band. Consequently, there are n pairs of complex conjugate roots, which ensure the presence of n frequencies in oscillations of $\langle\rho^n\rangle$. The frequencies ω_k are usually incommensurate, but their incommensurability vanishes in the deep of the allowed band at weak disorder. According to this picture, oscillations in $G(B)$ shown in Fig. 1 are determined by the superposition of incommensurate harmonics and their Fourier spectrum should contain discrete frequencies. This picture is indirectly confirmed by the experimental data obtained in [10] and cited in [8], according to which the distribution function $P(\rho)$ is not stationary, but demonstrates systematic aperiodic variations. [1]

It is clear from the above that the Fourier analysis of the function $G(B)$ makes it possible to establish

[1] It can be established by contradiction: if $P(\rho)$ were stationary, then all moments of conductance would be constant; in fact, its two first moments reveal aperiodic oscillations.

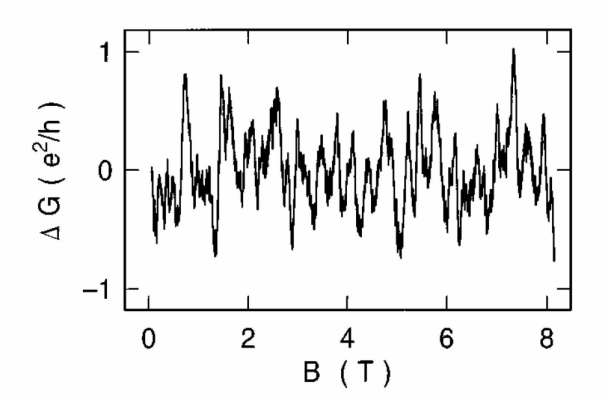

Figure 1: Magnetic field dependence of the conductance of the thin Au wire [5].

which of two scenarios is true. However, the dependence $G(B)$ shown in Fig. 1 cannot be used directly because a sharp cutoff of experimental data results in the appearance of slowly decaying oscillations in its Fourier transform and chaotization of the spectrum [2]. To obtain explicit results, it is necessary to use an appropriate smoothing function.

Let the function $f(x)$ be the superposition of discrete harmonics and be real. Then,

$$f(x) = \sum_k A_k \mathrm{e}^{i\omega_k x} = \frac{1}{2}\sum_k \left[A_k \mathrm{e}^{i\omega_k x} + A_k^* \mathrm{e}^{-i\omega_k x}\right] , \tag{3}$$

where the frequencies ω_k can be considered as positive without loss of generality. Then, the Fourier transform of $f(x)$ has the form

$$F(\omega) = \pi \sum_k \left[A_k \delta(\omega + \omega_k) + A_k^* \delta(\omega - \omega_k)\right] , \tag{4}$$

and its modulus

$$|F(\omega)| = \pi \sum_k |A_k| \left[\delta(\omega + \omega_k) + \delta(\omega - \omega_k)\right] \tag{5}$$

depends only on the intensities of spectral lines and does not contain information on phase shifts in the corresponding harmonics. Since $|F(\omega)|$ is an even function, it is possible to consider only positive ω values and to omit the first delta function in Eq. (5).

[2] Figure 14 in [5] shows the Fourier spectrum of a thin wire in comparison with the spectrum of a small ring; the latter contains additional oscillations caused by the Aharonov–Bohm effect. However, aperiodic oscillations were not discussed in this place and their spectrum, which is chaotic because of the sharp cutoff, was roughly approximated by the authors in the form of the envelope of oscillations. This is obvious from comparison with Figs. 12 and 13 in [5], where chaotic oscillations are clearly seen.

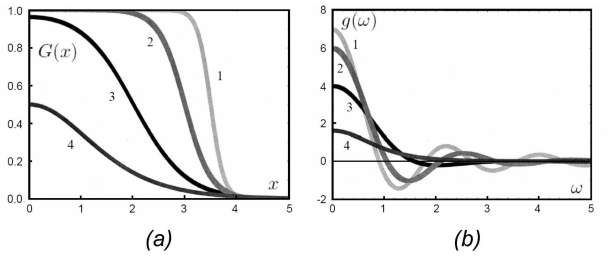

Figure 2: (a) Function $G(x)$ given by Eq. (9) and (b) its Fourier transform $g(\omega)$ at (1) $\mu = 3.5$, $T = 0.125$; (2) $\mu = 3$, $T = 0.25$; (3) $\mu = 2$, $T = 0.5$; and (4) $\mu = T \ln 2$, $T = 0.8$.

Since the function $f(x)$ can be experimentally measured only in a certain finite x range, we in practice have

$$f(x) = \frac{1}{2}\sum_k \left[A_k \mathrm{e}^{i\omega_k x} + A_k^* \mathrm{e}^{-i\omega_k x}\right] G(x) , \tag{6}$$

where the function $G(x)$ is unity within the working range and zero beyond it; further, it will be smoothed. Then, instead of Eq. (4), we obtain

$$F(\omega) = \frac{1}{2}\sum_k \left[A_k g(\omega + \omega_k) + A_k^* g(\omega - \omega_k)\right] , \tag{7}$$

where $g(\omega)$ is the Fourier transform of $G(x)$, which is real for even function $G(x)$. Thus, the restriction of the working range leads to the replacement of delta functions by spectral lines with finite widths. If discrete frequencies are well separated and the function $g(\omega)$ is strongly localized near zero, one can neglect the overlapping of functions $g(\omega \pm \omega_k)$ and write at positive frequencies

$$|F(\omega)|^2 \approx \frac{1}{4}\sum_k |A_k|^2 g^2(\omega - \omega_k) . \tag{8}$$

It is preferable to use the function $|F(\omega)|^2$ (so-called power spectral density [11]) because the integral of this function over all frequencies is equal to the integral of $f^2(x)$ over all x values. Consequently, change in the spectrum of $f(x)$ at fixed rms fluctuations results in the redistribution of intensities between different frequencies at the conservation of the total spectral power.

It is easy to see that, to obtain a clear picture in the case of a discrete spectrum, it is necessary to have a possibly narrower shape of spectral lines determined by $g(\omega)$, which can be achieved by the appropriate choice of the function $G(x)$. The general strategy is determined by the properties of integrals of rapidly oscillating functions [12]. If the function $f(x)$ has discontinuity, its Fourier transform decreases at high frequencies as $1/\omega$; if the nth derivative is discontinuous, then $F(\omega) \sim \omega^{-n-1}$. The Fourier transform of a smooth function $f(x)$ is calculated by shifting the contour of integration to a complex plane and is determined by the nearest singularity or saddle point, which leads to the dependence $F(\omega) \sim \exp(-\alpha\omega)$. If the regular function is obtained by means of a weak smoothing of a singularity, the α value is small and the exponential is manifested only at very high frequencies, whereas the behavior corresponding to the singularity holds in the remaining region. In our case, it is necessary to smooth the discontinuity of $G(x)$. It should be clear that weak smoothing is inefficient, while strong smoothing leads to small values of $G(x)$ near the boundaries of the working range and to loss of experimental information; so, a reasonable compromise is required.

Let $G(x)$ be the x-symmetrized Fermi function

$$G(x) = \frac{1}{1 + \mathrm{e}^{(x-\mu)/T} + \mathrm{e}^{(-x-\mu)/T}} = \\ = \frac{1}{1 + 2\mathrm{e}^{-\mu/T}\cosh(x/T)}\,, \qquad (9)$$

whose Fourier transform is given by the integral

$$g(\omega) = \int\limits_{-\infty}^{\infty} \frac{\mathrm{e}^{i\omega x}\,dx}{b\cosh\beta x + c} = \frac{2\pi}{b\beta\sinh x_0}\frac{\sin(\omega x_0/\beta)}{\sinh(\omega\pi/\beta)}\,,$$

$$x_0 = \operatorname{arccosh}(c/b)\,. \qquad (10)$$

If $x = B - \mu_0$ is chosen in our case, experimental data correspond to the interval $|x| \le \mu_0$ with $\mu_0 = 4$ (in units of tesla). We accepted $\mu = \mu_0 - 4T$, which ensures the small value $G(\mu_0) \approx 0.02$ at boundaries of the interval. As clear from Fig. 2, the behavior $g(\omega) = 2\sin\mu\omega/\omega$ characteristic of the sharp cutoff prevails at small T values (lines 1 and 2). It seems reasonable to choose $\mu = 2$ and $T = 0.5$ (line 3); in this case, 50% of experimental data are effectively used, while the lineshape is approximately the same as in the case of $\mu = T\ln 2$, where $x_0 = 0$, $g(\omega) = 2\pi T^2\omega/\sinh\pi T\omega$ and oscillations disappear completely (line 4).

The spectral analysis of experimental data (Fig. 1) was produced by calculation of the Fourier integral in the region $|x| < \mu_0$ with the indicated smoothing function. The corresponding results are shown in Fig. 3. The spectrum obviously consists of discrete lines, which confirms the second scenario given in beginning [3]. However, the spectrum in the range $\omega \lesssim 2\pi/\xi_B$ (where ξ_B was estimated as the average distance between neighboring maxima or minima in Fig. 1) [4] is similar to discrete white noise: in a rough approximation, the lines are equidistant and their intensities are more or less the same. Since the sum over frequencies is often approximated by an integral, discrete white noise does not differ in many properties from continuous white noise. Let, for example,

$$F(\omega) = \pi\sum_k \left[A_k\delta(\omega + \omega_k) + A_k^*\delta(\omega - \omega_k)\right] H(\omega)\,, \qquad (11)$$

where the frequencies ω_k are equidistant ($\omega_k = k\Delta$), the amplitudes A_k are the same in modulus ($|A_k| = A$) and have completely random phases, while $H(\omega)$ is an even function restricting the spectrum to the range $|\omega| \lesssim \Omega$. Then, determining $f(x)$ by means of the inverse Fourier transform, we obtain the correlation function

$$\langle f(x)f(x')\rangle = \frac{1}{2}\sum_k A^2H^2(\omega_k)\mathrm{e}^{i\omega_k(x-x')} \approx \\ \approx \frac{1}{2}A^2\Delta^{-1}h(x-x')\,, \qquad (12)$$

where $h(x)$ is the Fourier transform of $H^2(\omega)$. If the function $H(\omega)$ is smooth, $h(x)$ decreases exponentially at a scale of Ω^{-1} in agreement with the diagrammatic results obtained in [1–4].

In fact, a thin wire is a quasi-1D system, where the transverse motion is quantized, so a set of discrete levels ϵ_s^0 arise. If the longitudional movement along the x axis is taken into account, the levels transform to 1D subbands with the spectra

[3] The number and intensity of lines suggest that four first moments of ρ are really important, the fifth moment is less significant, while the higher moments are practically irrelevant.

[4] Under processing, Fig. 1 was strongly magnified and digitized by hand. It was revealed that sharp spikes in Fig. 1 are due to vertical dashes indicating uncertainty of the data, whereas the experimental dependence is in fact smooth.

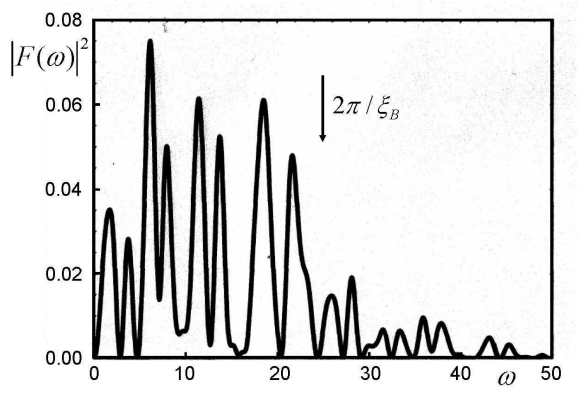

Figure 3: Fourier analysis of the experimental data shown in Fig. 1 with the smoothing function (9) at $\mu = 2$, $T = 0.5$.

$\epsilon_s(k_x) = \epsilon_s^0 + k_x^2/2m$, whose states are filled below the Fermi level. The magnetic field B affects most strongly the upper filled subband with the minimal Fermi energy ϵ_F, restricting the movement in it by the length L determined by the condition $m\omega_B^2 L^2 \sim \epsilon_F$, where $\omega_B = eB/mc$. The system conductance is determined by the sum of the subband conductances, whose oscillations are exponentially decreasing for large L. The main contribution to oscillations is given by the upper subband where the length L is minimal. The amplitude of oscillations has the order of e^2/h, in agreement with experiment and diagrammatic estimates [1–4].

In conclusion, the results obtained in this work reconcile two alternative scenarios described at the beginning. On the one hand, the spectrum is discrete, confirming the second scenario, where aperiodic conductance oscillations are due to the superposition of incommensurate harmonics. On the other hand, the spectrum as a whole resembles discrete white noise, which is close in properties to continuous white noise. Universal conductance fluctuations are discussed in a lot of works (see [13–33] and references therein), and it would be interesting to process another experimental data in the spirit of the present paper.

Appendix. **Derivation of Eq. (2)**

Let us consider the one-dimensional Anderson model specified by the discrete Schrödinger equation

$$\Psi_{n+1} + \Psi_{n-1} + V_n \Psi_n = E\Psi_n \,, \qquad (A.1)$$

where E is the energy measured from the center of the band, V_n are independent random variables with zero mean and variance W^2, while the hopping integral is taken to be unity. Rewriting Eq. (A.1) in the form

$$\begin{pmatrix} \Psi_{n+1} \\ \Psi_n \end{pmatrix} = \begin{pmatrix} E - V_n & -1 \\ 1 & 0 \end{pmatrix} \begin{pmatrix} \Psi_n \\ \Psi_{n-1} \end{pmatrix} , \quad (A.2)$$

and performing n iterations, one can easily obtain

$$\begin{pmatrix} \Psi_{n+1} \\ \Psi_n \end{pmatrix} = \begin{pmatrix} \tau_{11} & \tau_{12} \\ \tau_{21} & \tau_{22} \end{pmatrix} \begin{pmatrix} \Psi_1 \\ \Psi_0 \end{pmatrix} . \qquad (A.3)$$

Here, the matrix $\tau = ||\tau_{ij}||$ is the product of n matrices of the form (A.2) and satisfies an obvious recurrence relation, which can be represented in terms of matrix elements,

$$y_{n+1} = (E - V_n)y_n + z_n \,, \qquad z_{n+1} = -y_n \,, \quad (A.4)$$

where $y_n = \tau_{12}^{(n-1)}$, $z_n = \tau_{11}^{(n-1)}$ or $y_n = \tau_{22}^{(n-1)}$, $z_n = \tau_{21}^{(n-1)}$. It is substantial that $y^{(n-1)}$ and $z^{(n-1)}$ do not contain the quantity V_n and can be averaged independently of it. Setting $w_n^{(1)} = \langle y_n^2 \rangle$, $w_n^{(2)} = \langle y_n z_n \rangle$, $w_n^{(3)} = \langle z_n^2 \rangle$ for the second moments, one can easily come to the equation

$$\begin{pmatrix} w_{n+1}^{(1)} \\ w_{n+1}^{(2)} \\ w_{n+1}^{(3)} \end{pmatrix} = \begin{pmatrix} E^2 + W^2 & 2E & 1 \\ -E & -1 & 0 \\ 1 & 0 & 0 \end{pmatrix} \begin{pmatrix} w_n^{(1)} \\ w_n^{(2)} \\ w_n^{(3)} \end{pmatrix} , \quad (A.5)$$

Its solution is exponential, $w_n^{(i)} \sim \lambda^n$, where λ is an eigenvalue of the matrix. Setting $\lambda = 1 + x$, it is easy to obtain an equation for x, which has the following form in the limit of the continuous Schrödinger equation:

$$x\left(x^2 + 4\mathcal{E}\right) = 2W^2 \qquad (A.6)$$

where $\mathcal{E}$ is the energy measured from the band edge. The equation for the growth exponent of the fourth moments can be obtained similarly:

$$x\left(x^2 + 4\mathcal{E}\right)\left(x^2 + 16\mathcal{E}\right) = 42W^2x^2 + 96W^2\mathcal{E} \,. \quad (A.7)$$

The structure of equations for arbitrary $2n$th moments can be established using argumentation presented in Section 4 in [8], where a slightly different formalism was used. Deep in the allowed and forbidden bands, only diagonal elements can be retained in matrices (43) and (47) in [8] and their analogs

for higher moments. As a result, we arrive at the equation

$$\prod_{k=0}^{2n} \left[x + 2(n-k)\delta - B_n^k \epsilon^2\right] = O(\epsilon^4)\,, \qquad (A.8)$$

where $\epsilon^2 = W^2/4\mathcal{E}$, $\delta^2 = -\mathcal{E}$, $B_n^k = n(2n–1)+3k(k–2n)$. A similar equation near the band edge

$$x^{2n+1} = \sum_{k=0}^{k_{max}} C_k W^{2k} x^{2n+1-3k}\,, \quad k_{max} = \left[\frac{2n+1}{3}\right] \qquad (A.9)$$

follows from observation that all terms of the equation have the same order of magnitude at $x \sim \delta \sim \epsilon^2$ and only combinations $\delta^{2n}\epsilon^{2m}$ with $n \geq m$ are allowed, among which only $\delta^{2n}\epsilon^{2n} \sim W^{2n}$ remain finite at $\delta \to 0$.

Landauer resistance ρ is determined by a quadratic form of the matrix elements τ_{ij} [8]. Consequently, growth exponents for $\langle\rho^n\rangle$ coincide with those for the $2n$th moments of τ_{ij}. An expression for $\langle\rho^n\rangle$ contains a linear combination of the corresponding exponents, which leads to Eq. (2) if the complex-valued exponents are taken into account.

References

[1] Lee P A and Stone A D 1985 Universal Conductance Fluctuations in Metals *Phys. Rev. Lett.* **55**, 1622–1625.

[2] Lee P A, Stone A D and Fukuyama H 1987 Universal conductance fluctuations in metals: Effects of finite temperature, interactions, and magnetic field *Phys. Rev.* B **35**, 1039–1069.

[3] Altshuler B L 1985 Fluctuations in the extrinsic conductivity of disordered conductors *JETP Lett.* **41**, 648–651.

[4] Altshuler B L and Khmelnitskii D E 1985 Fluctuation properties of small conductors *JETP Lett.* **42**, 359–363.

[5] Washburn S and Webb R A 1986 Aharonov-Bohm effect in normal metal quantum coherence and transport *Adv. Phys.* **35**, 375-422.

[6] Beenakker C W J 1997 Random-matrix theory of quantum transport *Rev. Mod. Phys.* **69**, 731–808.

[7] Efetov K B 1995 *Supersymmetry in disorder and haos* (Cambridge, University Presss).

[8] Suslov I M 2019 Conductance distribution in 1D systems: dependence on the Fermi level and the ideal leads *J. Exp. Theor. Phys.* **129**, 877-895.

[9] Landau L D, Lifshitz E M 1977 *Quantum Mechanics* (Pergamon).

[10] Mailly D and Sanquer M 1992 Sensitivity of quantum conductance fluctuations and of 1/f noise to the time reversal symmetry *J. Phys.* (France) I **2**, 357–364.

[11] Press W H, Flannery B P, Teukolsky S A and Wetterling W T 1992 *Numerical Recipes in Fortran* (Cambridge University Press).

[12] Migdal A B 1975 *Qualitative Methods in Quantum Theory* (Nauka, Moscow).

[13] Hals K M D, Nguyen A K, Waintal X and Brataas A 2010 Effective Magnetic Monopoles and Universal Conductance Fluctuations *Phys. Rev. Lett.* **105**, 207204.

[14] Lien A S, Wang L Y, Chu C S and Lin J J 2011 Temporal universal conductance fluctuations in RuO2 nanowires due to mobile defects *Phys. Rev.* B **84**, 155432.

[15] Ramos J G G S, Bazeia D, Hussein M C and Lewenkopf C 2011 Conductance Peaks in Open Quantum Dots *Phys. Rev. Lett.* **107**, 176807.

[16] Li Z et al 2012 Two-dimensional universal conductance fluctuations and the electron-phonon interaction of surface states in Bi2Te2Se microflakes *Sci. Rep.* **2**, 595.

[17] Rossi E, Bardarson J H, Fuhrer M S and Sarma S D 2012 Universal Conductance Fluctuations in Dirac Materials in the Presence of Long-range Disorder *Phys. Rev. Lett.* **109**, 096801.

[18] Yang P Y, Wang L Y, Hsu Y W and Lin J J 2012 Universal conductance fluctuations in indium tin oxide nanowires *Phys. Rev.* B **85**, 085423.

[19] Minke S, Bundesmann J, Weiss D and Eroms J 2012 Phase coherent transport in graphene nanoribbons and graphene nanoribbon arrays *Phys. Rev.* B **86**, 155403.

[20] Gustavsson S, Bylander J and Oliver W D 2013 Time-Reversal Symmetry and Universal Conductance Fluctuations in a Driven Two-Level System *Phys. Rev. Lett.* **110**, 016603.

[21] Barbosa A L S, Hussein M S and Ramos J G G S 2013 Anticorrelation for conductance fluctuations in chaotic quantum dots *Phys. Rev.* E **88**, 010901(R).

[22] Jacquod Ph and Adagideli I 2013 Universal features of spin transport and breaking of unitary symmetries *Phys. Rev.* B **88**, 041305(R).

[23] Bundesmann J, Liu M H, Adagideli I and Richter K 2013 Spin conductance of diffusive graphene nanoribbons: A probe of zigzag edge magnetization *Phys. Rev.* B **88**, 195406.

[24] Richardson C L et al 2015 Vortex detection and quantum transport in mesoscopic graphene Josephson-junction arrays *Phys. Rev.* B **91**, 245418.

[25] Vasconcelos T C, Ramos J G G S and Barbosa A L R 2016 Universal spin Hall conductance fluctuations in chaotic Dirac quantum dots *Phys. Rev.* B **93**, 115120.

[26] Kalmbach C C et al 2016 Nonequilibrium mesoscopic conductance fluctuations as the origin of 1/f noise in epitaxial graphene *Phys. Rev.* B **94**, 205430.

[27] Ramos J G G S, Barbosa A L R, Carlson B V, Frederico T and Hussein M S 2016 Correlation functions and correlation widths in quantum-chaotic scattering for mesoscopic systems and nuclei *Phys. Rev.* E **93**, 012210.

[28] Hu Y, Liu H, Jiang H and Xie X C 2017 Numerical study of universal conductance fluctuations in three-dimensional topological semimetals *Phys. Rev.* B **96**, 134201.

[29] Hsu H C, Kleftogiannis I, Guo G Y and Gopar V A 2018 Conductance Fluctuations in Disordered 2D Topological Insulator Wires: From Quantum Spin-Hall to Ordinary Phases it J. Phys. Soc. Jpn **87**, 034701.

[30] Aamir M A et al 2018 Marginally Self-Averaging One-Dimensional Localization in Bilayer Graphene *Phys. Rev. Lett.* **121**, 136806.

[31] Islam S et al 2018 Universal conductance fluctuations and direct observation of crossover of symmetry classes in topological insulators *Phys. Rev.* B **97**, 241412R.

[32] Vercosa T, Doh Y J, Ramos J G G S and Barbosa A L R 2018 Conductance peak density in nanowires *Phys. Rev.* B **98**, 155407.

[33] Hajiloo F, Hassler F and Splettstoesser J 2019 Mesoscopic effects in the heat conductance of superconducting-normal-superconducting and normal-superconducting junctions *Phys. Rev.* B **99**, 235422.